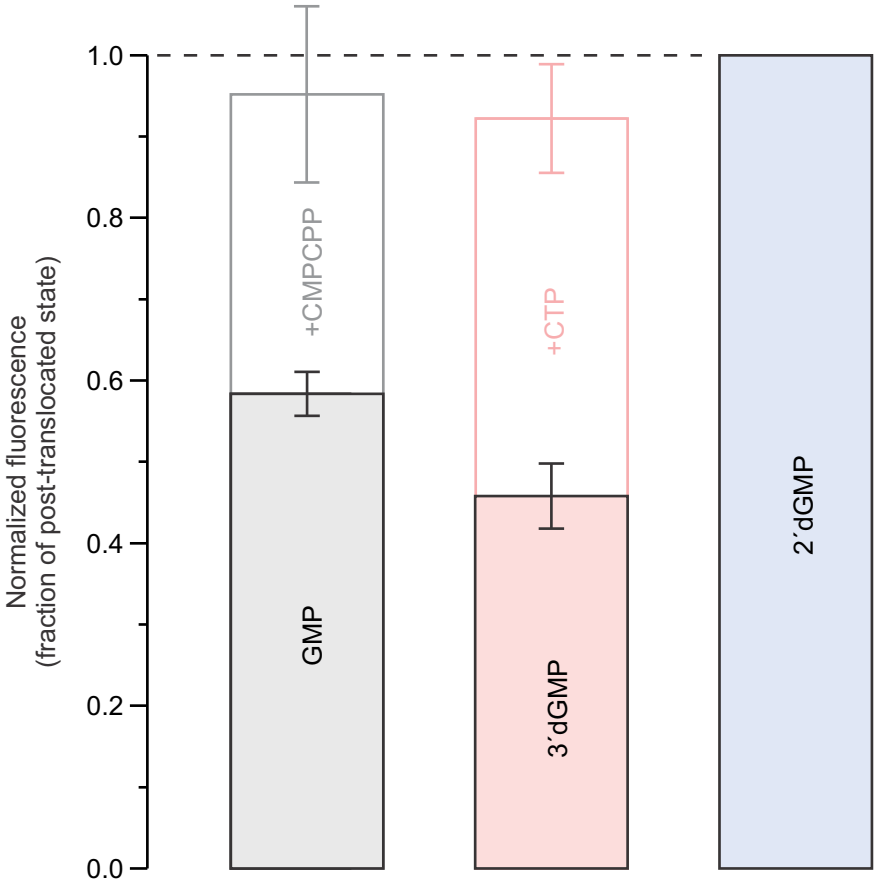

Supplementary Figure 1: β'P750L TECs display measurable fractions of the pre-translocated state. Fluorescence of rNMP (grey fill) and 3'dNMP (pink fill) extended TECs normalized to the level of 2'dNMP extended TECs (pastel blue fill). White bars depict the effects of the next substrate NTP (pink outline) or its nonhydrolyzable analogue (grey outline). Error bars are SDs of three independent experiments.

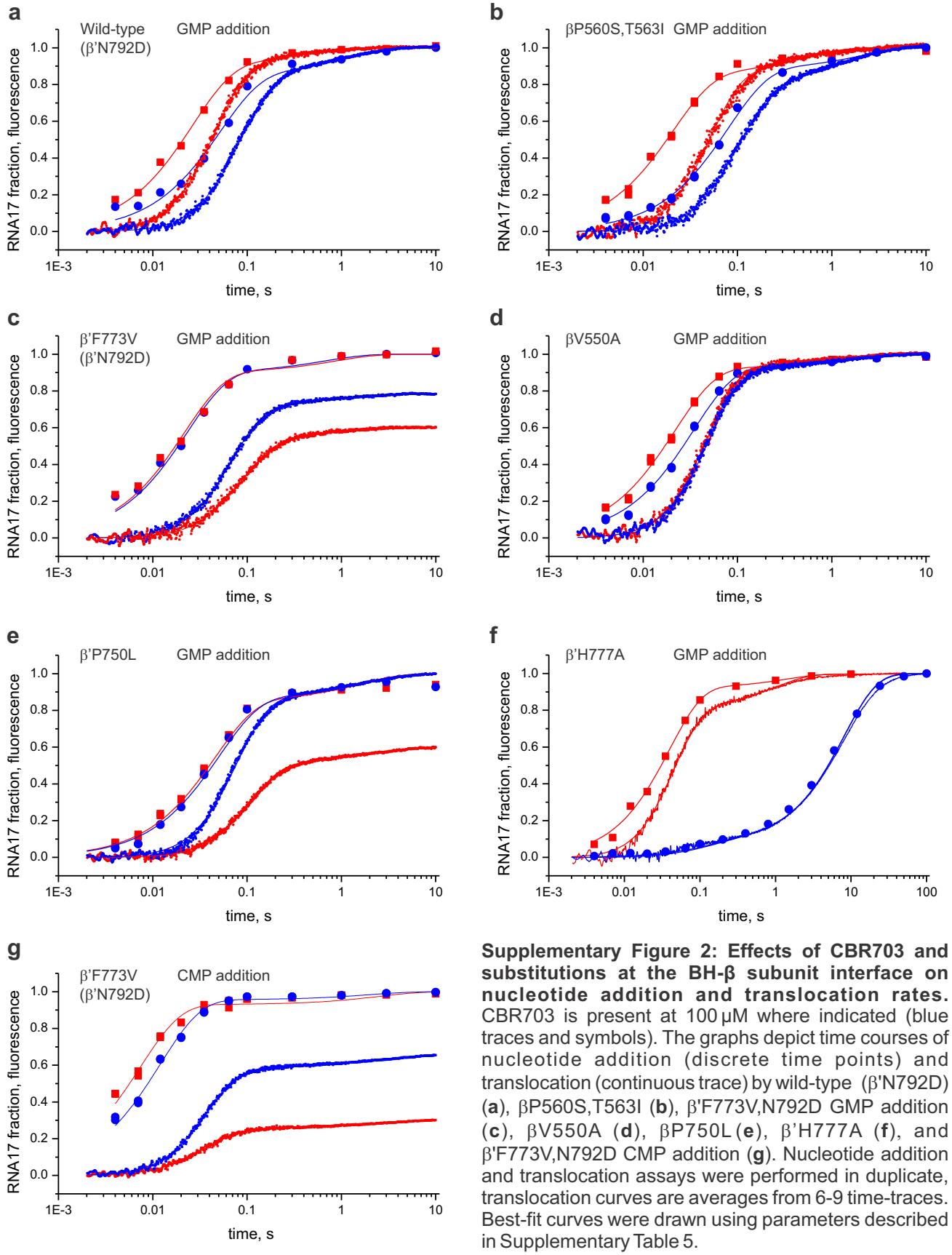

Supplementary Figure 2: Effects of CBR703 and substitutions at the BH-β subunit interface on nucleotide addition and translocation rates. CBR703 is present at 100 μM where indicated (blue traces and symbols). The graphs depict time courses of nucleotide addition (discrete time points) and translocation (continuous trace) by wild-type (β'N792D) (**a**), βP560S,T563I (**b**), β'F773V,N792D GMP addition (**c**), βV550A (**d**), βP750L (**e**), β'H777A (**f**), and β'F773V,N792D CMP addition (**g**). Nucleotide addition and translocation assays were performed in duplicate, translocation curves are averages from 6-9 time-traces. Best-fit curves were drawn using parameters described in Supplementary Table 5.

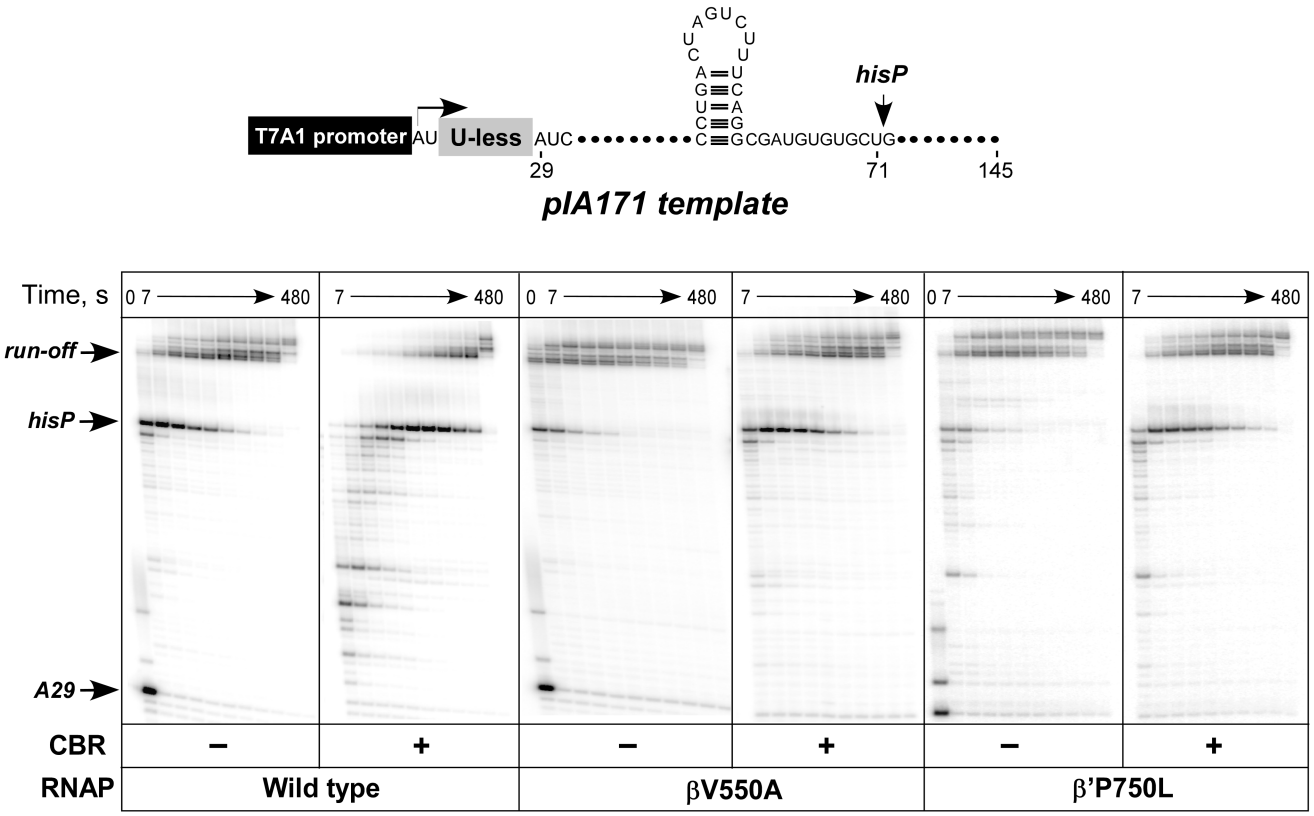

Supplementary Figure 3: **Effects of CBR703 and substitutions at the BH-β subunit interface on pausing at the regulatory pause site.** Transcript elongation on pIA171 template by wild-type, βV550A and β'P750L RNAPs in the absence (*left panels*) or in the presence (*right panels*) of 100 μM CBR703. Quantification of the fraction of RNA at the *hisP* (transcript position U71) is shown in Fig. 4b. Each assay was performed in triplicate.

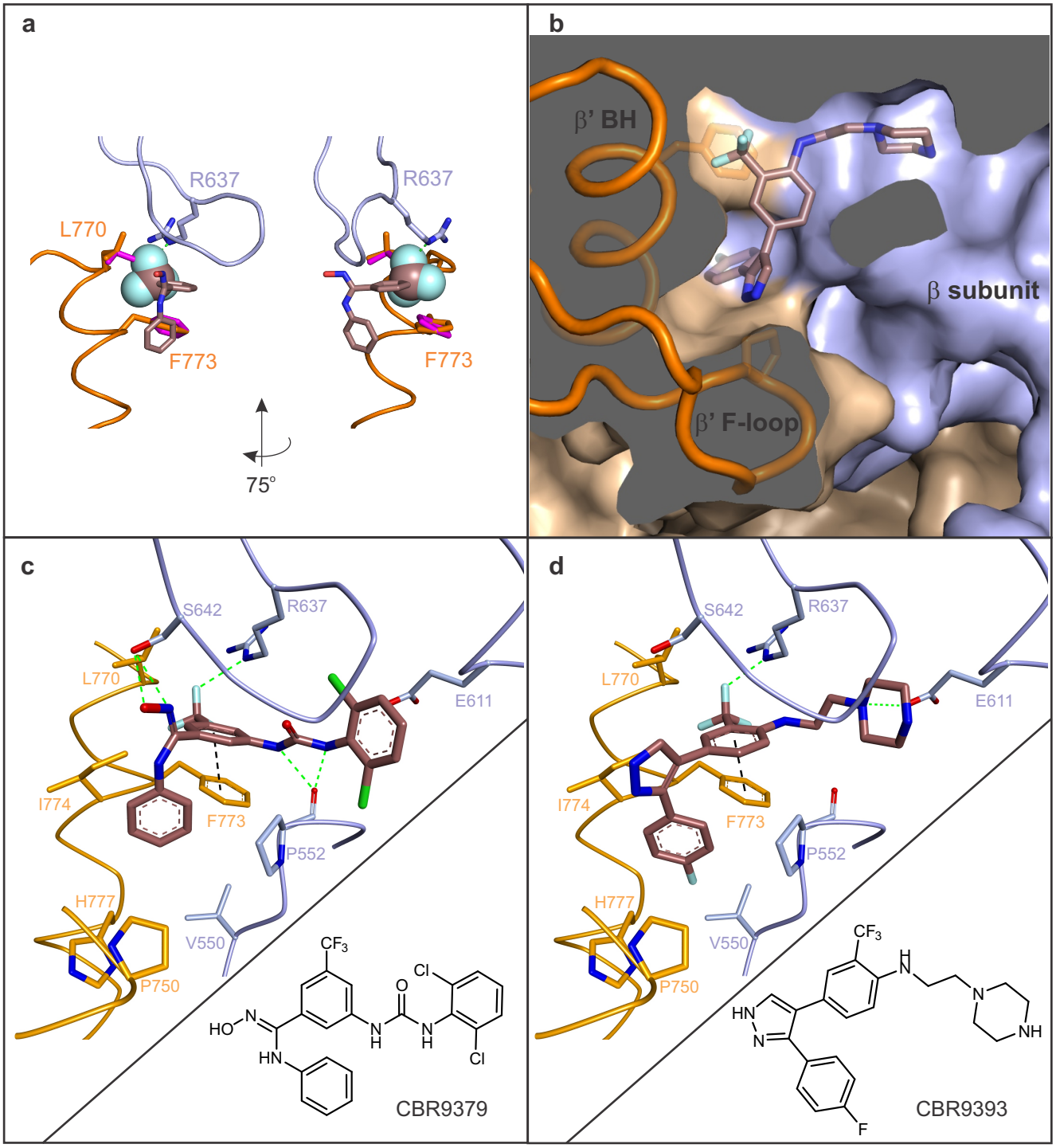

Supplementary Figure 4: Binding site of CBR series inhibitors at the BH-β subunit interface. (**a**) Adjustments of β'Leu770 and β'Phe773 side chain positions were essential for recovery of a common binding mode for CBR703, CBR9379 and CBR9393. Trifluoromethyl group is depicted as spheres, the rest of CBR703 as sticks (brown carbons), selected elements of β (pastel blue) and β' (orange) subunits are represented by cartoons. The original conformations (PDB 4IGC) of β'Leu770 and β'Phe773 side chains are depicted as magenta sticks. (**b**) CBR binding cavity: β (pastel blue) and β' (orange) subunits are depicted as surfaces, BH and F-loop as orange cartoons, β'P750, β'F773 side chains (orange carbons) and CBR9393 (brown carbons) as sticks. (**c, d**) Best scoring (lowest negative binding energy) poses recovered for CBR9379 (**c**) and CBR9393 (**d**) by both GOLD and AutoDock Vina. Color coding as in main article Fig. 1b. Green and black dashed lines depict polar and π-stacking interactions, respectively. 2D structures of inhibitors are presented in insets. Figure was prepared using PyMOL Molecular Graphics System, Version 1.6.0.0 Schrödinger, LLC (**a**, **b**) and Discovery Studio 3.5 (Accelrys) (**c**, **d**). The sources of atomic coordinates are listed in Supplementary Table 3.

S041M-R024: GMP addition, Fig. 2, 3, 5, Supplementary Fig. 1, 2

S048M-R024: CMP addition, Fig. 2, 3, Supplementary Fig. 2

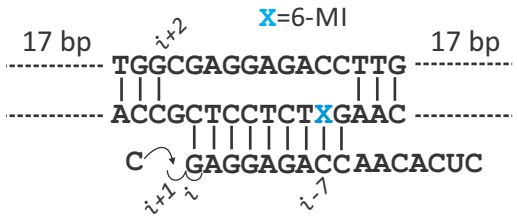

S056M-R024: AMP addition, Fig. 2a

S058M-R024: UMP addition, Fig. 2a

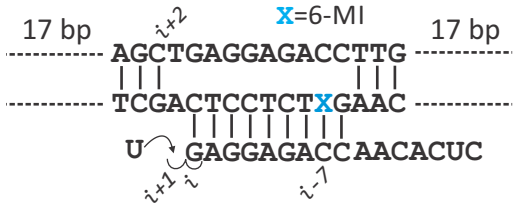

Supplementary Figure 5: Nucleic acid components of TECs used in this study. In Fig. 2 and Supplementary Fig. 1 the assembled TEC16s are extended by one nucleotide and the effects of low molecular weight ligands on fluorescence of TEC17s are studied. In Fig. 3, 5 and Supplementary Fig. 2 both the nucleotide incorporation by TEC16 and translocation of the extended, product TEC17s are resolved in time.

Supplementary Table 1. *E. coli* RNAP expression vectors used in this study

Name	Description	Source/reference
pVS10	wild-type (T7p-α-β-β'_His_6-T7p-ω)	Ref. 2
pVS48	β'F773V (T7p-α-β-β'[F773V]_His_6-T7p-ω)	Ref. 3
pTG003	β'F773V,N792D (T7p-α-β-β'[F773V,N792D]_TEV_His_{10}-T7p-ω)	this work
pTG004	β'N792D (T7p-α-β-β'[N792D]_TEV_His_{10}-T7p-ω)	this work
pTG007	β'H777A (T7p-α-β-β'[H777A]_TEV_His_{10}-T7p-ω)	this work
pTG012	β'P750L (T7p-α-β-β'[P750L]_TEV_His_{10}-T7p-ω)	this work
pAM022	βV550A (T7p-α-His_6_β[V550A]-β'-ω)	this work
pAM023	βP560S,T563I (T7p-α-His_6_β[P560S,T563I]-β'-ω)	this work

Maps and sequences of the plasmids are available upon request.

Supplementary Table 2. Template strand DNA oligonucleotides and RNA primers used in this study

Name	Substrate	Sequence (5'→3')	Employment
S041M	GTP	GCTACTCTACTGACATGATGCCTCCTCT**X**GAACCTTAGATCGCTACAAGT	Fig. 2, 3, 5, Suppl. Fig. 1, 2
S048M	CTP	GCTACTCTACTGACATGACCGCTCCTCT**X**GAACCTTAGATCGCTACAAGT	Fig. 2, 3, Suppl. Fig. 2
S056M	ATP	GCTACTCTACTGCAATGACGTCTCCTCT**X**GAACCTTAGATCGCTACAAGT	Fig. 2a
S058M	UTP	GCTACTCTACTGCAATGTCGACTCCTCT**X**GAACCTTAGATCGCTACAAGT	Fig. 2a
R024	-	Atto680-CUCACAACCAGAGGAG	Fig. 2, 3, 5, Suppl. Fig. 1, 2

X = 6-methyl-isoxanthopterin (6-MI)

Sequences that base-pair with RNA in the initial TECs are underlined.

Supplementary Table 3. The sources of atomic coordinates used to prepare Fig. 1, 6 and Supplementary Fig. 4

Figure	RNAP	RNA&DNA	Ligand(s)
Fig. 1a	*T. thermophilus* TEC (PDB ID 2O5J), lineage specific domain (β'132-456) omitted	*E. coli* TEC model, Ref. 1	none
Fig. 1b	*E. coli* holoenzyme PDB 4IGC, conformations of β'Leu770 and β'Phe773 altered (Suppl. Fig. 4a)	none	CBR703 docked with AutoDock Vina
Fig. 6a	*T. thermophilus* TEC (PDB ID 2O5J), lineage specific domain (β'132-456) omitted	*E. coli* TEC model. Ref. 1	none
Fig. 6b	*T. thermophilus* TEC (PDB ID 2O5J), lineage specific domain (β'132-456) omitted	*E. coli* TEC model, Ref. 1	CBR703 docked with AutoDock Vina Myxopyronin (PDB ID 3EQL) Rifapentin (PDB ID 2A69) Streptolydigin (PDB ID 2PPB)
Suppl. Fig. 4a	*E. coli* holoenzyme PDB 4IGC, altered and original conformations of β'Leu770 and β'Phe773	none	CBR703 docked with AutoDock Vina
Suppl. Fig. 4b	*E. coli* holoenzyme PDB 4IGC conformations of β'Leu770 and β'Phe773 altered (Suppl. Fig. 4a)	none	CBR9393 docked with AutoDock Vina. GOLD recovered very similar pose.
Suppl. Fig. 4c	*E. coli* holoenzyme PDB 4IGC, conformations of β'Leu770 and β'Phe773 altered (Suppl. Fig. 4a)	none	CBR9379 docked with GOLD. AutoDock Vina recovered very similar pose.
Suppl. Fig. 4d	*E. coli* holoenzyme PDB 4IGC, conformations of β'Leu770 and β'Phe773 altered (Suppl. Fig. 4a)	none	CBR9393 docked with AutoDock Vina. GOLD recovered very similar pose.

Supplementary Table 4. Parameters describing titrations of TEC17s with TGT, CBR703, STL and CMPCPP

Fig.	RNAP	template	3' NMP	L	L2	K_L, μM	$F^{TEC17\cdot L}$ (normalized)
2b	β'F773V,N792D	S041M	GMP	CMPCPP		9±2	0.85 ±0.05
2b	β'F773V,N792D	S041M	GMP	TGT		0.027 ±0.003	0
2b	β'F773V,N792D	S041M	GMP	CBR703		47 ±14	0.88 ±0.13
2b	β'F773V,N792D	S048M	CMP	CBR703		28 ±7	0.75 ±0.15
2b	β'F773V,N792D	S048M	CMP	STL		0.24 ±0.13	1.0 ±0.1
2c	β'N792D	S041M	GMP	TGT		0.055 ±0.007	0
2c	β'N792D	S041M	GMP	TGT	100 μM CBR703	0.36 ±0.05	0.25 ±0.09
2c	β'N792D	S041M	GMP	TGT	0.75 μM STL	0.28 ±0.04	0.2 ±0.1
2c	β'N792D	S041M	GMP	STL	0.1 μM TGT	0.97 ±0.13	1 ±0.1
2c	β'N792D	S041M	GMP	CBR703	0.1 μM TGT	7.0 ±1.5	0.78 ±0.08

Errors are standard deviations of the best fit estimates for parameters and were calculated by nonlinear regression of the 6-MI fluorescence intensities versus L concentration using model for fitting equilibrium titration data described on page 8 of Supplementary Information.

Supplementary Table 5. Parameters describing kinetics of nucleotide addition and translocation (Fig. 3, Supplementary Fig. 2)

Figures	RNAP	substrate	CBR703	k_{c+1}	k_{t+1}	k_{t-1}	k_{i+1}	k_{i-1}
Fig. 3a, 3c, Suppl. Fig. 2a	β'N792D	GTP		36 ±2 (28-49)	56 ±3 (41-73)	0	3.3 ±0.3 (1.6-6.6)	0.35 ±0.06 (0.1-1.1)
Fig. 3a, 3c, Suppl. Fig. 2a	β'N792D	GTP	100 μM	18 ±1 (14-23)	30 ±2 (24-42)	0	1.0 ±0.1 (0.8-1.5)	0.18 ±0.01 (0.1-0.3)
Fig. 3c, Suppl. 2b	βP560S,T563I	GTP		56 ±2 (45-62)	29 ±1 (26-37)	0	2.3 ±0.2 (1.2-4.8)	0.40 ±0.06 (0.2-1.2)
Fig. 3c, Suppl. Fig. 2b	βP560S,T563I	GTP	100 μM	16 ±1 (10-17)	26 ±1 (23-50)	0	0.9 ±0.1 (0.6-1.3)	0.26 ±0.02 (0.1-0.4)
Fig. 3b, 3c, Suppl. 2c	β'F773V, N792D	GTP		49 ±2 (44-55)	8.2 ±0.2 (7.2-9.4)	5.4 ±0.2 (4.8-6.4)	1.5 ±0.2 (0.5-3.6)	0.18 ±0.04 (0.04-0.7)
Fig. 3b, 3c, Suppl. Fig. 2c	β'F773V, N792D	GTP	100 μM	46 ±2 (39-55)	15.8 ±0.4 (14-18)	4.4 ±0.1 (4.0-5.1)	1.4 ±0.2 (0.6-3.5)	0.14 ±0.02 (0.04-0.5)
Fig. 3c, Suppl. Fig. 2d	βV550A	GTP		46 ±2 (39-54)	36 ±1 (32-42)	0	1.0 ±0.1 (0.4-2.4)	0.07 ±0.01 (0.03-0.2)
Fig. 3c, Suppl. Fig. 2d	βV550A	GTP	100 μM	31 ±1 (28-35)	52 ±2 (44-60)	0	0.7 ±0.1 (0.4-1.5)	0.06 ±0.01 (0.03-0.1)
Fig. 3c, Suppl. Fig. 2e	β'P750L	GTP		22 ±1 (21-26)	9.3 ±0.2 (8.8-10)	6.4 ±0.1 (6-7)	0.6 ±0.1 (0.4-1)	0.11 ±0.01 (0.07-0.17)
Fig. 3c, Suppl. Fig. 2e	β'P750L	GTP	100 μM	20 ±1 (18-24)	34 ±2 (28-39)	0	0.6 ±0.1 (0.5-0.7)	0.09 ±0.01 (0.06-0.12)
Fig. 3c, Suppl. Fig. 2g	β'F773V, N792D	CTP		143 ±3 (133-156)	8.8 ±0.2 (8.2-9.4)	21.0 ±0.4 (20-23)	0.5 ±0.1 (0.2-1.0)	0.07 ±0.01 (0.03-0.1)
Fig. 3c, Suppl. Fig. 2g	β'F773V, N792D	CTP	100 μM	86 ±2 (79-94)	23.0 ±0.3 (22-24)	12.4 ±0.2 (12-13)	0.5 ±0.1 (0.3-0.7)	0.05 ±0.01 (0.03-0.08)
Fig. 3c, Suppl. Fig. 2f	β'H777A	GTP		30 ±1 (26-37)	72 ±4 (54-91)	0	1.1 ±0.1 (0.9-1.6)	0.23 ±0.02 (0.2-0.4)
Fig. 3c, Suppl. Fig. 2f	β'H777A	GTP	100 μM	Not applicable. See fitting of nucleotide addition and translocation as a function of [CBR703] on page 10 of Suppl. Information				

Errors are standard deviations of the best fit estimates for parameters and were calculated by nonlinear regression of the 6-MI fluorescence and RNA17 band intensities versus time using model for fitting of nucleotide addition and translocation data described on page 9 of Supplementary Information. Values in parentheses indicate lower and upper bounds of parameters calculated at a 10% increase in Chi^2 over the minimal value using FitSpace routine of Kintek Explorer.

Supplementary Methods

Data normalization (applies to all fluorescence data in this study)

Equilibrium levels of fluorescence of extended TECs (TEC17s) were extrapolated to 100% incorporation efficiency, the TEC16 fluorescence was subtracted, and the resulting value was normalized to that of 2'dNMP extended TECs. For example, for GMP extended TEC normalization was performed as follows:

$$\text{Normalized fluorescence of TEC17} = \frac{\frac{\text{Fluorescence of GMP extended TEC17}}{\text{GMP incorporation efficiency}} - \text{Fluorescence of TEC16}}{\frac{\text{Fluorescence of 2'dGMP extended TEC17}}{\text{2'dGMP incorporation efficiency}} - \text{Fluorescence of TEC16}}$$

Model employed for fitting equilibrium titration data (Fig. 2, Supplementary Table 4)

System of equations:

$$F = F^{TEC17\cdot L} \times TEC17\cdot L - F^{TEC17} \times (TEC17_{total} - TEC17\cdot L)$$

$$K_L = \frac{(TEC17_{total} - TEC17\cdot L) \times (L_{total} - TEC17\cdot L)}{TEC17\cdot L}$$

Constrains:

$$0 < TEC17\cdot L < TEC17_{total}$$
$$0 < TEC17\cdot L < L_{total}$$
$$0 < K_L$$

Independent variables: L_{total}, total ligand concentration

Dependent variables:

F -Fluorescence of 6-MI base in TEC17

Parameters:

K_L - equilibrium constant of ligand (L) binding

F^{TEC17} -normalization coefficient (fluorescence of unligated TEC17)

$F^{TEC17\cdot L}$ -normalization coefficient (fluorescence of ligand saturated TEC17)

Model employed for fitting of nucleotide addition and translocation data (Fig. 3, Supplementary Fig. 2 and Supplementary Table 5)

Initial conditions (See Note 1):

T=0 A = p (~0.2) B = 1-p (~0.8) C = 0 D = 0

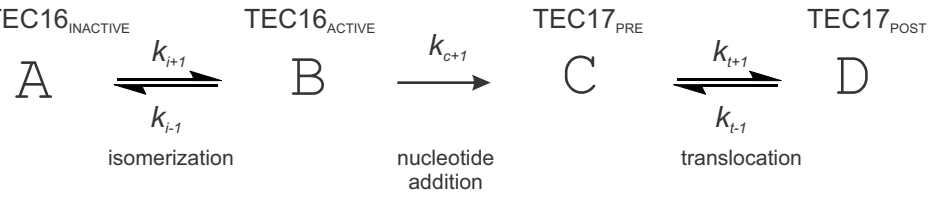

Rate equations (See Note2):

$A' = -A*k_{i+1}+B*k_{i-1}$

$B' = -B*k_{c+1} - B*k_{i-1} + A*k_{i+1}$

$C' = -C*k_{t+1} + B*k_{c+1} + D*k_{t-1}$

$D' = -D*k_{t-1} + C*k_{t+1}$

Equations for dependent variables:

RNA17=F1*(C+D)

SF_fluorescence=F2*(A+B+C)+F3*D

Independent variables: T -time

Dependent variables:
RNA17 -RNA17 band intensities from quench flow experiment
SF_fluorescence -Fluorescent trace from stopped-flow experiment

Parameters:
k_{i+1} -rate of isomerization of inactive TEC into active TEC
k_{i-1} -rate of isomerization of active TEC into inactive TEC
k_{c+1} -rate of nucleotide incorporation
k_{t+1} -rate of forward translocation
k_{t-1} -rate of backward translocation (See Note 3)

F1 -normalization coefficient for quench flow data
F2 -normalization coefficient for stopped-flow data (See Note 4)
F3 -normalization coefficient for stopped-flow data (See Note 4)
p -fraction of inactive TEC (See Note 1)

Note 1: The fraction of inactive TEC (”p” parameter) is determined by k_{i+1} and k_{i-1} because TEC16 is assembled and reaches equilibrium in the absence of NTP. To reflect this condition we introduced a 100 s mixing step without NTP into the Kintek Explorer virtual experiment setup. The initial fractions of active and inactive TEC16 can then be chosen arbitrary, the ”p” parameter is redundant and is not explicitly used.

Note 2: Rate equations are uniquely defined by the reaction scheme and do not need to be explicitly specified when fitting data with Kintek Explorer.

Note 3: k_{t-1} was fixed to zero for all but β’F773V datasets and β’P750L dataset without CBR703.

Note 4: F2, F3 were allowed to vary when k_{t-1} is fixed to zero (all but β’F773V datasets and β’P750L dataset without CBR). When k_{t-1} was allowed to vary (β’F773V datasets and β’P750L dataset without CBR) the data were pre-normalized and F2, F3 were constrained based on the equilibrium levels of fluorescence of extended TECs (Fig. 2 and Supplementary Fig. 1).

Fitting of nucleotide addition and translocation data as a function of [CBR703] (Fig. 5 and Supplementary Fig. 2f)

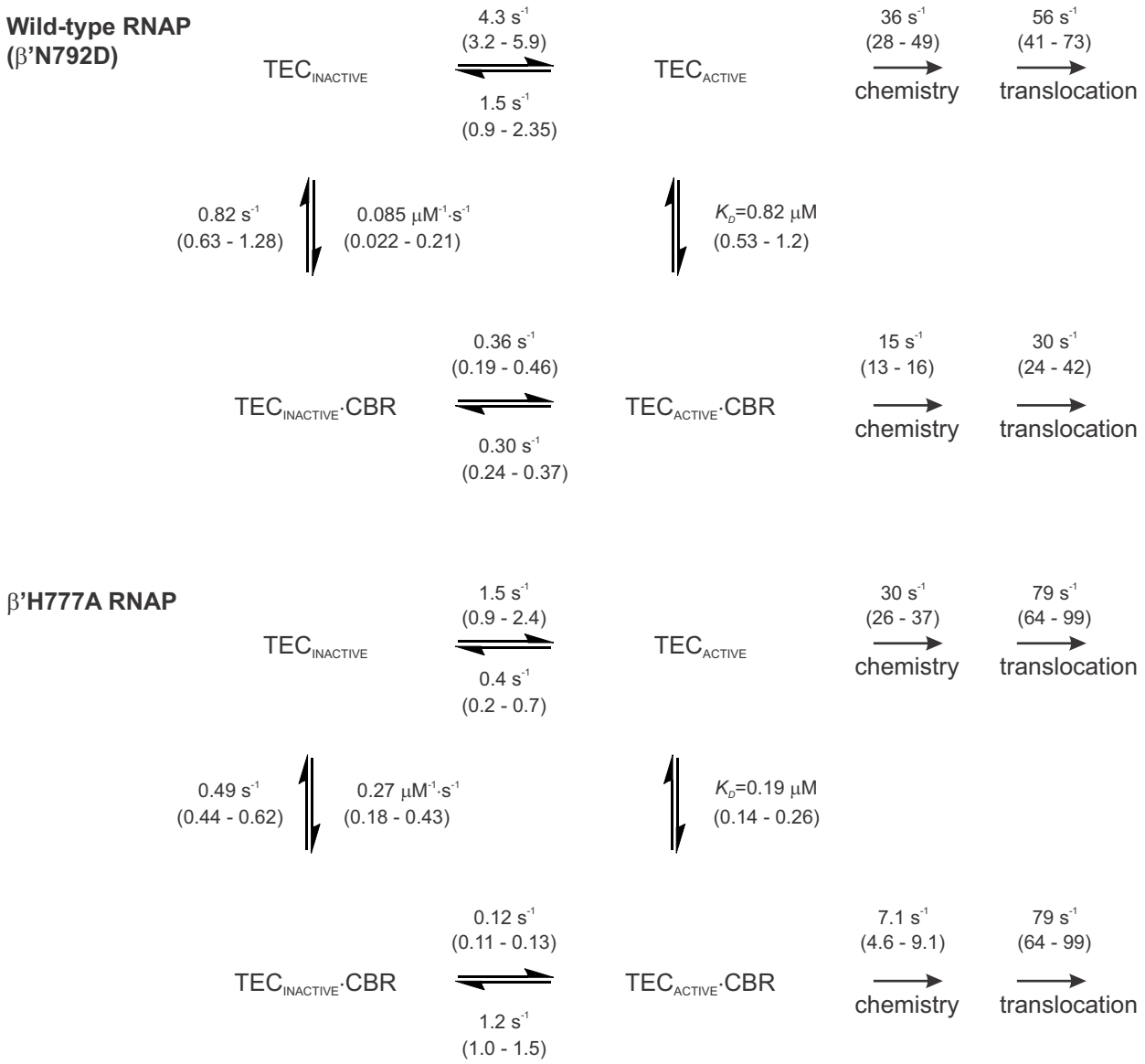

Values in parentheses indicate lower and upper bounds of parameters calculated at a 10% increase in Chi^2 over the minimal value using FitSpace routine of Kintek Explorer

Supplementary References

1. Opalka, N. et al. Complete structural model of *Escherichia coli* RNA polymerase from a hybrid approach. *PLoS Biol.* **8**, doi: 10.1371/journal.pbio.1000483 (2010).

2. Belogurov, G. A. et al. Structural basis for converting a general transcription factor into an operon-specific virulence regulator. *Mol. Cell* **26**, 117–129 (2007).

3. Svetlov, V., Belogurov, G. A., Shabrova, E., Vassylyev, D. G. & Artsimovitch, I. Allosteric control of the RNA polymerase by the elongation factor RfaH. *Nucleic Acids Res.* **35**, 5694–5705 (2007).